IEEE Access
Multidisciplinary ⋮ Rapid Review ⋮ Open Access Journal

Received 4 November 2024, accepted 12 December 2024, date of publication 25 December 2024, date of current version 3 January 2025.

Digital Object Identifier 10.1109/ACCESS.2024.3522204

RESEARCH ARTICLE

Improved Motion Correction in Dynamic Contrast-Enhanced MRI Using Low Rank With Soft Weighting

JICHANG ZHANG[1,2], FAISAL NAJEEB[3], YULIN WANG[1], XINPEI WANG[4], PENGFEI XU[5], HAMMAD OMER[3], JIANJUN ZHENG[6,7], JINGFENG ZHANG[6,7], SUE FRANCIS[8], PAUL GLOVER[8], RICHARD BOWTELL[8], THOMAS MEERSMANN[8], AND CHENGBO WANG[1,9]

[1]Faculty of Science and Engineering, University of Nottingham, Ningbo 315100, China
[2]XinGaoYi Medical Equipment Company Ltd., Yuyao 315400, China
[3]MIPRG Research Group, Department of Electrical and Computer Engineering, COMSATS University Islamabad, Islamabad 45550, Pakistan
[4]Philips Healthcare Technology (China) Company, Suzhou Branch, Suzhou 215000, China
[5]Hebei Key Laboratory of Intelligent Data Information Processing and Control, Tangshan University, Tangshan 063000, China
[6]Ningbo Clinical Medical Research Center of Imaging Medicine, Ningbo 315010, China
[7]Ningbo No. 2 Hospital, Ningbo 315010, China
[8]Sir Peter Mansfield Imaging Centre, University of Nottingham, NG7 2RD Nottingham, U.K.
[9]Nottingham Ningbo China Beacons of Excellence Research and Innovation Institute, Ningbo 315040, China

Corresponding author: Chengbo Wang (chengbo.wang@nottingham.edu.cn)

This work was supported in part by XGY Medical Equipment Company, Yuyao, China; in part by the National Key Research and Development Program of China under Grant 2022YFC2408900; in part by Ningbo "S&T Innovation 2035" Major Programs under Grant 2020Z079, Grant 2022Z141, and Grant 2023Z182; and in part by Ningbo Clinical Research Center for Medical Imaging under Grant 2021L003.

ABSTRACT This paper introduces a motion-corrected, free-breathing dynamic contrast-enhanced (DCE) MRI reconstruction method, termed low-rank plus sparse (L+S) with soft weighting. We designed a soft weighting matrix that smoothly transitions spokes between the target and other motion states to suppress motion blurring. The optimized fast iterative shrinkage-thresholding algorithm (FISTA) was employed to solve the L+S optimization problem, enabling faster convergence and better image quality. A DCE-MRI computer simulation framework, based on a modified Shepp-Logan model, was used as ground truth to quantify the motion suppression errors. Both simulation and clinical datasets demonstrate that the proposed method provides superior motion correction, higher temporal resolution, and over 5 times faster reconstruction speed than existing motion-corrected GRASP frameworks.

INDEX TERMS Compressed sensing, DCE-MRI, motion correction, parallel imaging, reconstruction efficiency, soft weighting.

I. INTRODUCTION

Dynamic contrast-enhanced (DCE) MRI induces significant signal intensity changes in tissues by the injected contrast agent. Tumors and normal tissues exhibit distinct signal variation curves [1], [2], [3], [4], making DCE-MRI a powerful tool for detecting tumors and other lesions [5], [6]. Achieving high spatio-temporal resolution is crucial to accurately capture tissue's dynamic signal variation. Multiple three-dimensional (3D) images are required to be rapidly acquired in different dynamic phases, which poses significant challenges to MRI systems.

Over the past decades, various reconstruction frameworks have been developed for DCE-MRI to reconstruct highly under-sampled datasets. Golden Angle Radial Sparse Parallel (GRASP) combines the acceleration ability of parallel imaging and compressed sensing to achieve a high acceleration factor (AF) in reconstruction [7], [8]. It employs a stack-of-stars golden-angle radial sampling pattern to achieve fast and uniform 3D k-space coverage. The acquired spokes are

The associate editor coordinating the review of this manuscript and approving it for publication was Marco Giannelli.

evenly subdivided into multiple time frames according to acquisition time order [9]. GRASP explores the temporal incoherence across these time frames and recovers the image series with excellent quality.

However, the spokes within a single time frame may be acquired at different motion states. Although the stack-of-stars sampling pattern provides enhanced motion robustness, periodic respiratory and cardiac motions remain challenging for DCE-MRI, often leading to motion blurring [10], [11].

To further reduce motion blurring in DCE-MRI, motion-corrected GRASP techniques, such as extra-dimension (XD) GRASP [12] and respiratory-weighted (RACER) GRASP [13], were developed. Both XD-GRASP and RACER-GRASP introduce additional motion state subdivisions within each time frame, providing additional motion state information for DCE-MRI [14], [15], [16], [17]. XD-GRASP reconstructs multiple motion states simultaneously, while RACER-GRASP combines motion states with different weighting factors to lock a desired motion state. However, this motion state subdivision increases the under-sampling ratio. XD-GRASP struggles with reconstruction at high temporal resolution due to excessive AF [13], whereas RACER-GRASP achieves better reconstruction quality at high temporal resolution by using a weighted combination of motion states. Nevertheless, RACER-GRASP shows worse motion suppression when reconstructing the intermediate motion state.

Meanwhile, reconstruction of the additional motion state increases the computation burden of both XD-GRASP and RACER-GRASP [18], [19]. Although self-calibrating GRAPPA operator gridding (GROG) has been implemented to accelerate the reconstruction, the computation cost remains challenging for clinical applications [16], [20].

Beyond these two motion-resolved GRASP methods, various motion-resolved methods, such as MostMco [21] and MoCoLoR [22], have been developed. However, these methods primarily focus on dynamic MRI reconstruction and are associated with a higher computation burden. Alternative motion correction approaches in DCE-MRI including motion registration, outlier spokes removal, and increasing temporal resolution, etc., have also been explored [23], [24], [25], [26], [27]. However, these methods cannot provide adequate motion state information and may compromise acquisition efficiency.

Low rank plus sparse (L+S) decomposition is a widely used model for DCE-MRI reconstruction, providing improved tissue contrast and temporal fidelity, especially at high AF reconstruction [28], [29], [30]. L+S decomposition employs an iterative shrinkage-thresholding algorithm (ISTA) [31] to obtain the optimal solution, significantly enhancing reconstruction efficiency compared to NLCG in GRASP-based methods by reducing the number of gridding and de-gridding procedures. Hence, combining L+S decomposition with motion-resolved techniques is a promising approach for improving the motion-corrected DCE-MRI reconstruction.

In this work, we developed a motion-resolved DCE-MRI reconstruction method by incorporating a soft-weighting matrix into the standard L+S decomposition model, termed "L+S with soft-weighting,". This approach preserves high reconstruction efficiency, enhances motion suppression, and provides rich motion state information for DCE-MRI simultaneously. A modified fast ISTA (FISTA) algorithm [31] is used to recover motion-resolved images from the proposed model efficiently. Additionally, a computer simulation framework was developed to evaluate the performance of different reconstruction schemes. Further details about this research can be found in the author's Ph.D. thesis [32].

II. METHODS

The proposed "L+S with soft weighting" method extends L+S decomposition by incorporating an additional motion suppression mechanism. The goal of the proposed method is to establish a new free-breathing DCE-MRI reconstruction framework, as illustrated in Figure 1, which provides merits that include time-efficient reconstruction, enhanced motion suppression, and flexible motion resolution simultaneously.

A. MOTION ESTIMATION AND MOTION CORRECTED GRASP

The stack-of-stars golden angle radial sampling scheme repeatedly acquires the central k-space line along the partition dimension which can present the projection profiles of the object during the scanning. By applying the principal components analysis (PCA) algorithm [33] to evaluate these projection profiles, the motion signal can be estimated without the need for external gating devices [15].

Based on the estimated motion signal, the radial spokes within each time frame are resorted according to their respiratory displacement. XD-GRASP bins these resorted spokes into four different motion states, and the motion-resolved images are reconstructed by solving the following optimization problem:

$$argmin_x = \frac{1}{2}\|Ex - d\|_2^2 + \lambda_T \|TV_T x\|_1 + \lambda_M \|TV_M x\|_1 \tag{1}$$

where E is the multi-coil encoding operator with a number of c coil field maps followed by an under-sampled non-uniform fast Fourier Transform (NUFFT) operator, x is the image series with additional motion state dimension to be reconstructed, d is acquired the c-coil dataset. TV_T and TV_M are total variation (TV) operators applied on the temporal and motion state dimensions with corresponding penalty factors λ_T and λ_M, respectively. XD-GRASP provides additional rich motion state information at the cost of reduced temporal resolution and reconstruction efficiency.

Like the XD-GRASP, RACER-GRASP subdivides the resorted spokes in each time frame into four motion states. The difference is that it explores the sparsity of each

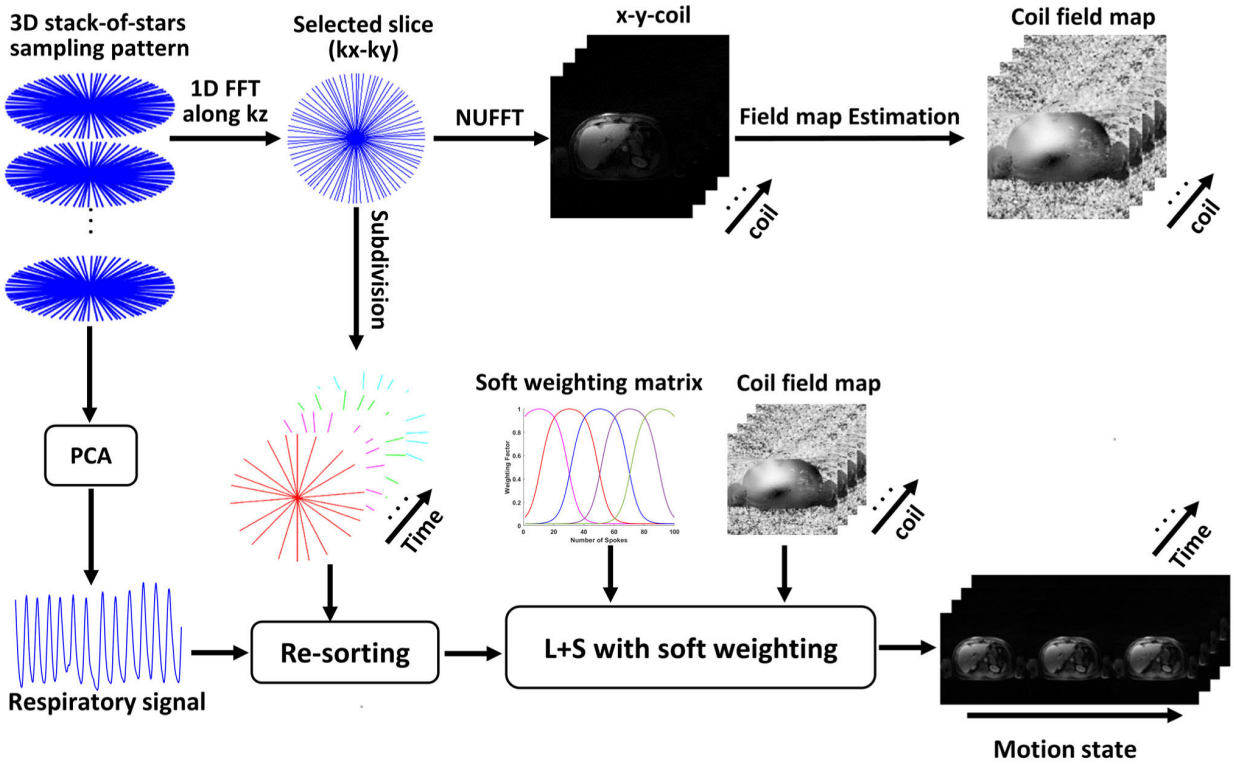

FIGURE 1. L+S with soft weighting reconstruction framework. 3D dynamic MRI datasets are typically acquired by the stack-of-stars hybrid sampling pattern. A one-dimensional (1D) FFT operator is applied on the kz dimension to decompose the 2D slices' k-space from the 3D datasets. NUFFT is directly implemented for the composite k-space dataset before the time frame subdivision to obtain the reference images. Field maps are estimated using the Walsh algorithm [38] on the reference images. A respiratory motion signal is extracted from the repeatedly acquired k-space center along the slice dimension with PCA [15]. Continuously acquired k-space data are sorted into multiple time frames according to the temporal order and resorted further based on the respiratory motion signal. The soft weighting matrix directly assigns a specific weighting factor to each spoke to lock down the desired motion state. By shifting the weighting factor in the soft weighting matrix, the reconstructed image series provides additional motion dimension without the cost of temporal resolution.

motion state along the temporal dimension separately but not among these motion states. RACER-GRASP combines these reconstructed motion states with different weighting factors in the k-space domain as the final output.

$$argmin_x = \frac{1}{2} \|REx - d\|_2^2 + \lambda_T \|TV_T x\|_1 \qquad (2)$$

where R contains m motion weighting factors for a total of m respiratory motion states, R decayed exponentially from the desired motion state to other motion states. This delicate combination of motion states alleviates the computation burden caused by motion subdivision, while RACER-GRASP can support motion-corrected reconstruction at higher temporal resolution than XD-GRASP. Motion-resolved RACER-GRASP reconstruction can be achieved by switching the distribution of weighting factors in R.

B. L+S WITH SOFT WEIGHTING

L+S decomposition subdivides the acquired datasets into the low-rank components L and sparse components S [28], [29], [34]. L and S represent the steady background components and the dynamic varied components of the DCE-MRI dataset, respectively. By exploring the sparsity of S with an appropriate transform, a sparser representation of dynamic components can be achieved.

L+S converts the acquired dynamic dataset from the k-space domain into a space-time (y-t) matrix M. The row and column of M represent spatial pixel series and temporal series, respectively. A low-rank y-t matrix L is obtained by applying singular value decomposition (SVD) and singular value thresholding (SVT) on M. Another sparse y-t matrix S is derived by subtracting the original matrix M from the low-rank matrix L. L contains a limited number of non-zero singular values, while S contains a few non-zero entries. Due to the compressed background information, S shows better sparsity than the original matrix on y-t space, which benefits compressed sensing reconstruction. Like GRASP-based frameworks, L+S decomposition adopted temporal TV as the sparsity transform. Temporal TV applies a finite differences operator along the columns of the y-t matrix S. With a sparser representation of S, the number of sparse coefficients required for image recovery is reduced, allowing

dynamic MRI reconstruction at increased AF. The image series in the L+S decomposition can be obtained as:

$$argmin_{L,S} = \frac{1}{2}\|E(L+S)-d\|_2^2 + \lambda_L\|L\|_* + \lambda_T\|TV_T S\|_1 \quad (3)$$

where the nuclear norm $\|L\|_*$ and the l_1 norm $\|TV_T S\|_1$ present the sum of the singular values of the L and the sum of the absolute value of S's entries in the temporal TV domain, respectively. λ_L and λ_T are two penalty factors that trade off the data consistency versus the complexity of the solution given by the nuclear norm of L and the l_1 norm of S.

To achieve the motion-corrected L+S reconstruction, a soft weighting matrix W has been developed and integrated into the framework, forming L+S with soft weighting. The soft weighting matrix directly assigns a specific weighting factor to each motion-resorted spoke to lock down the desired motion state, eliminating additional motion state reconstruction and reducing the computation burden. The motion-corrected reconstruction can be achieved by solving the following problem using the proposed method.

$$argmin_{L,S} = \frac{1}{2}\|W\{E(L+S)-d\}\|_2^2 + \lambda_L\|L\|_* + \lambda_T\|TV_T S\|_1 \quad (4)$$

where W contains n weighting factors for a total of n spokes within each time frame.

RACER-GRASP binned the spokes within a time frame into four motion states and assigned an exponentially decayed weighting factor to these motion states. The R in RACER-GRASP induced a "stair-step" weighting matrix on spokes, as shown in Figure 2a. Hence, the weighting factors in R performed as a "hard bandpass" filter among resorted spokes, introducing abrupt weighting truncation for the spokes on motion dimension. Meanwhile, R provides a worse weighting factor distribution when reconstructing the intermediate motion state within the motion cycle.

To address these limitations in motion-corrected reconstruction, the weighting factors in W in the proposed method are generated by a modified sigmoid function. The modified sigmoid function enables a smooth transition between weighting factors for the spokes in the desired motion state and weighting factors for the spokes in other motion states, alleviating the unexpected truncation artifacts. The generation of W is mathematically expressed as:

$$W(t) = \frac{1}{1+e^{-t}} + C,\ t \in [n_1 n_2] \quad (5)$$

where n_1 and n_2 are two constants delicately designed to select certain segmentations of the sigmoid curve with a smooth but rapid transition among respiratory motion states. C is a constant of a small value so that all the spokes are involved in the iterative reconstruction, while the undersampling ratio and artifacts can be alleviated.

By accurately controlling the contribution from spokes acquired at different motion states during iterative reconstructions, improved motion suppression can be achieved by the soft weighting matrix than motion state subdivision. Apart from edge motion states, the soft weighting matrix provides good weighting factor distribution for feasible motion states by combining two opposite sigmoid functions, enabling effective motion suppression in reconstructing any motion states. By shifting the weighting factors in the soft weighting matrix, motion-resolved reconstruction can be achieved at high motion resolution without compromising temporal resolution.

TABLE 1. L+S with soft weighting and optimized FISTA for dynamic MRI reconstruction.

L+S with Soft Weighting Using Optimized FISTA
input:
d: multicoil undersampled k-t data
E: multicoil k-t encoding operator
W: motion weighting coefficient matrix
T: temporal total variation sparsity transform
λ_L: singular-value threshold
λ_T: sparsity threshold for temporal total variation
Initialize: $M_0 = Ed$, $R_1 = M_0$, $S_0 = 0$, $t_1 = 1$,
for $k = 1$ **to** K **do**
$L_k = SVT(R_k - S_{k-1})$
% soft thresholding in the temporal T domain
$S_k = T^{-1}(\Lambda_{\lambda_T}(T(R_k - L_{k-1})))$
if $k \le 2$ **do**
% Data consistency: subtract residual without W
$M_k = L_k + S_k - E^*((E(L_k + S_k) - d))$
else
% Data consistency: subtract residual with W
$M_k = L_k + S_k - E^*(W(E(L_k + S_k) - d))$
end if
% iteration for the step size
$t_{k+1} = (1 + \sqrt{1 + 4\,(t_k)^2}\,)/2$
% specific linear combination as the next input
$R_{k+1} = M_k + ((t_k - 1)/t_{k+1})(M_k - M_{k-1})$
end for
output: L, S

C. OPTIMIZED FAST ITERATIVE SHRINKAGE THRESHOLDING ALGORITHM

ISTA is used in the standard L+S decomposition model to solve the optimization problem. The convergence of ISTA can be further accelerated by combining the previous two iterative stages with specific coefficients, named FISTA. FISTA retains the computational simplicity characteristic of ISTA while improving convergence rates [35], [36], [37]. In this work, we applied FISTA to solve the proposed L+S model with the soft weighting matrix. W remains inactive during the initial two iterations to minimize the undersampling artifacts caused by the W.

Table 1 summarizes the optimized FISTA for solving the proposed model. Initially, the input image series matrix is subjected to an SVD operator as $M = U\Sigma V^H$. A soft thresholding operator Λ_λ is defined as $\Lambda_\lambda(x) = \frac{x}{|x|}\max(|x| - \lambda, 0)$, in which x and λ are a complex number and a real-valued threshold respectively. The SVT operator, a combination of Λ_λ and the SVD operator, is implemented

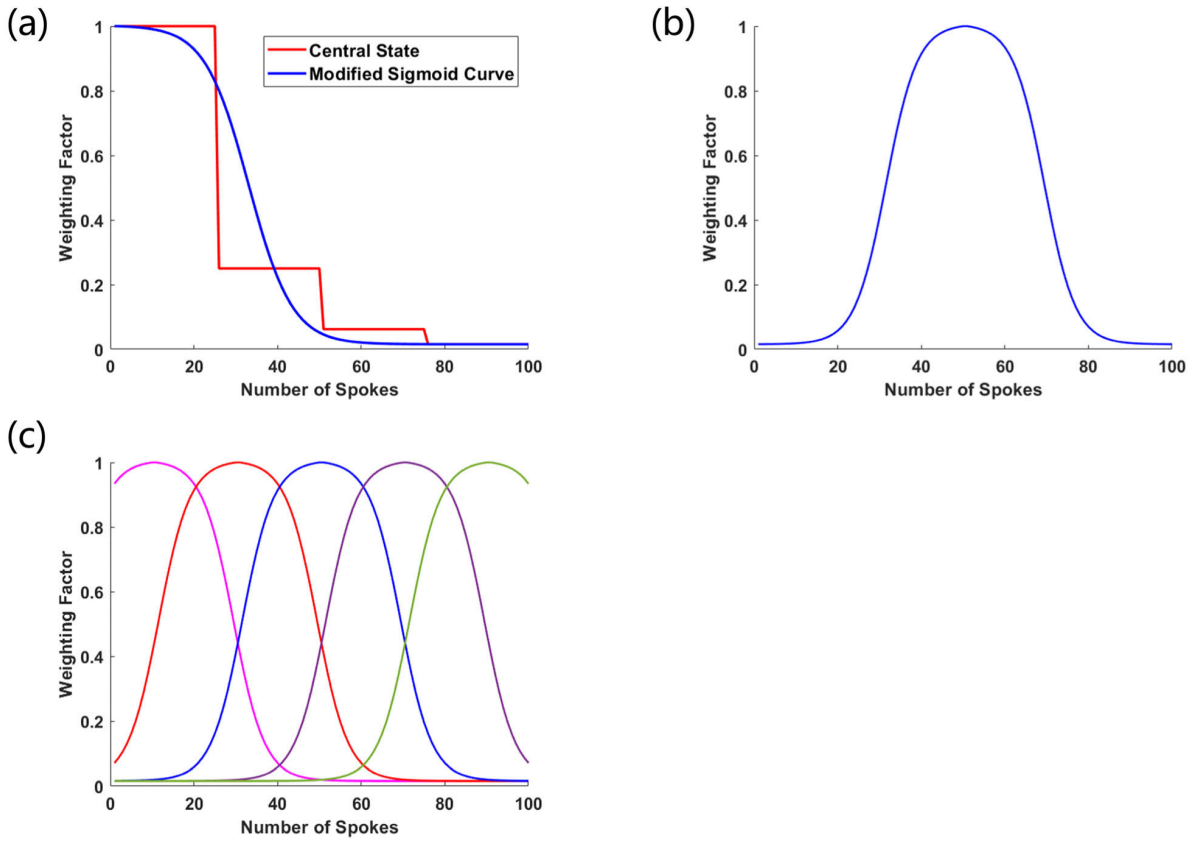

FIGURE 2. The weighting factor distribution of the RACER-GRASP and the proposed soft weighting matrix in a time frame with 100 spokes. (a) A comparison of the stair-step weighting function used in RACER-GRASP and the modified sigmoid function used in the soft weighting matrix on edge motion state. (b) The soft weighting matrix generated by combined sigmoid functions for reconstructing feasible motion states. (c) Shifting the weighting factor in the soft weighting matrix with a certain step size for reconstructing different motion states.

to process the singular value of M as $SVT_\lambda(M) = U\Lambda_\lambda(\Sigma)V^H$. After thresholding the singular value of M by Λ_λ, a low-rank matrix L is obtained. Based on the low-rank and sparse decomposition, the dynamic matrix S can be derived as $S = M - L$.

During the kth iteration of FISTA, the input image series R_k is generated by a specific linear combination of output image series M in the previous two iterations. The current low-rank matrix L_k is obtained by $SVT(R_k - S_{k-1})$, and the dynamic matrix S_k is obtained by $R_k - L_{k-1}$. To explore a sparser representation of the dynamic matrix, S_k is converted into the temporal TV transform domain and processed by another soft-thresholding operator Λ_{λ_T}. The ultimate kth sparse matrix is then recovered based on the remaining sparse coefficients as $S_k = T^{-1}(\Lambda_{\lambda_T}(T(R_k - L_{k-1})))$. The output image series M_k is figured out by subtracting $(L_k + S_k)$ with the residual aliasing artifacts weighted by the soft weighting matrix$W$ as $M_k = L_k + S_k - E^*(W(E(L_k + S_k) - d))$. W remains inactive during the initial two iterations to minimize the under-sampling artifacts.

The input image series for next iteration R_{k+1} is then created with a specific linear combination of current iteration output M_k and previous iteration output M_{k-1} as $R_{k+1} = M_k + ((t_k - 1)/t_{k+1})(M_k - M_{k-1})$, where t_k is an iteration step coefficient. $(t_k - 1)/t_{k+1})$ gradually reduces the contribution of M_{k-1} for the next iteration. The algorithm will proceed with iterations until the relative change in the solution falls below 10^{-5} or the maximum number of iterations is achieved.

This algorithm modified the effect of W in the first two iterations. The additional under-sampling artifacts caused by W can be minimized in the subsequent iteration. Due to the weighted contribution of spokes in the following iteration, the reconstructed image series M_k is gradually approaching the desired motion state. The optimized FISTA algorithm can suppress motion blurring and alleviate under-sampling artifacts simultaneously.

D. COMPUTER SIMULATION WORK

A computer simulation framework was developed to evaluate motion blurring for different reconstruction schemes, as shown in Figure 3. A two-dimensional (2D) modified Shepp-Logan phantom with 768 × 768 voxels was created, incorporating dynamic contrast variation and periodic rigid motion. The phantom consists of two static background sections and five dynamic sections. The gray levels of the two background sections were set to 1 and 0.2, respectively, and remained constant throughout the simulation, representing the tissues without contrast enhancement in DCE-MRI.

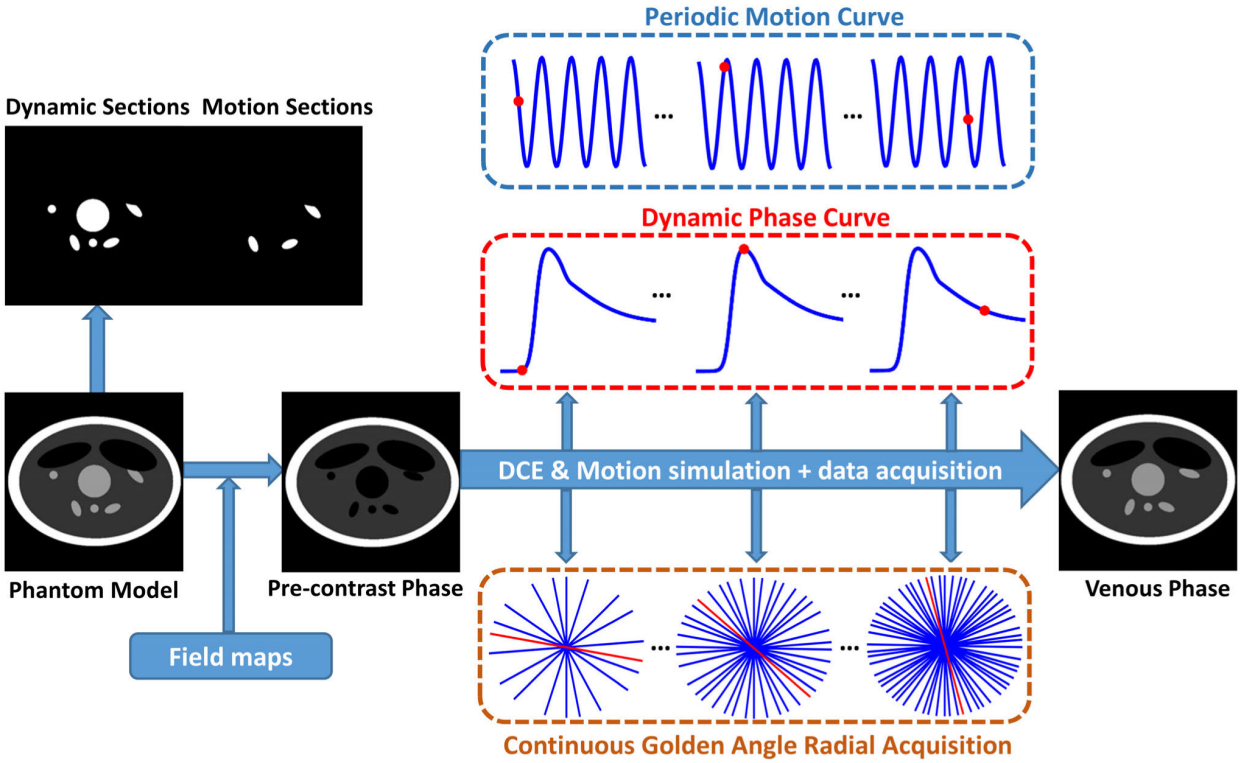

FIGURE 3. Flowchart of data acquisition during dynamic variation and rigid motion period. Eight field maps were integrated into phantom before data acquisition, forming multiple virtual coil channels. The simulation of data acquisition contains a total of 1100 steps between the pre-contrast phase and the venous phase. Two data acquisitions were executed at each time point, producing a fully sampled reference DCE series and a continuous DCE phantom dataset.

A dynamic variation curve was designed based on several clinical DCE-MRI datasets. The virtual duration of the curve is 157 s, with a peak at 32.9 s. The gray levels of the dynamic sections were initialized to 0 at the start of the simulation. Their signal intensity varied according to the dynamic curve, simulating the tissues with dynamic contrast enhancement in the DCE-MRI.

A periodic motion variation curve was also designed to accompany the dynamic variation curve. The virtual duration of the curve is 157 s, and includes 48 virtual respiratory cycles, simulating the respiratory motion at a rate of 18.3 cycles/minute. The motion degree of the curve model ranges from $-15°$ to $+15°$. Three dynamic sections were designated as motion sections, which rotated according to the motion curve, simulating tissues with both dynamic contrast enhancement and respiratory motion in DCE-MRI.

The Bloch equation simulation was performed using MATLAB 2022b (MathWorks, Natick, MA). During the simulation, the dynamic variation duration with respiratory motion was uniformly divided into 1100 discrete time steps, resulting in a time interval of approximately 0.14s. Additionally, eight exponentially decayed field maps were incorporated to systematically modulate the signal intensity of the phantom model on a pixel-by-pixel basis, thereby generating multiple virtual coil channels (c=8). T_2 decay was ignored while a homogeneity B_0field was assumed throughout the computer simulation.

E. DATA ACQUISITION

The phantom datasets were acquired using a golden-angle radial sampling pattern. A radial spoke is continuously acquired among these discrete time steps. The ultimately under-sampled dataset consists of eight virtual coils, a total of 1100 spokes across 1100 time steps, each containing 768 readout points. Subsequently, an average image, without subdivision into time frames, was directly reconstructed using a multi-coil NUFFT operator to estimate field maps.

A fully sampled k-space dataset was acquired at each discrete time point, simulating the reference k-space series. This fully sampled k-space dataset was acquired with 768 readout points and 1200 ($768 \times \pi/2$) spokes. Therefore, 1200×1100 spokes were generated for the reference datasets over the dynamic simulation period. The resulting matrix size for the reference series dataset was $768 \times 1200 \times 1100$, incorporating eight virtual coils.

A free-breathing liver DCE-MRI dataset provided by Feng [12] was utilized to evaluate the effectiveness of various

reconstruction schemes for motion suppression. This liver dataset was acquired from a healthy volunteer using a stack-of-stars golden angle FLASH pulse sequence. The acquisition parameters were as follows: TR/TE = 3.52 ms/1.41 ms, flip angle = 12°, FOV = 360 × 360 × 240 mm^3, number of partitions = 80, with 60% slice reduction and 6/8 partial Fourier applied along the slice dimension. The slice kspace dataset consists of twelve channels and 1100 spokes, each with 512 readout points. To prevent readout aliasing and gridding artifacts caused by NUFFT, oversampling was applied along the readout direction. The central 384 data points on each spoke were remained. After slice decomposition, the 2D liver dataset underwent coil unstreaking and coil compression before the reconstruction. This process reduced the dataset size from 384*1100*12 to 384*1100*8.

F. IMAGE RECONSTRUCTION

The phantom and liver datasets were subdivided into 11 frames with a temporal resolution of 100 spokes/frame (∼13s/frame). The corresponding AF is 12 for the phantom and 8 for liver datasets. The simulation dataset was reconstructed with a 512 × 512 × 11 matrix size by NUFFT, GRASP, XD-GRASP, RACER-GRASP, L+S decomposition, and L+S with soft weighting, respectively. The liver dataset was reconstructed using NUFFT, GRASP, XD-GRASP, RACER-GRASP, and L+S with soft weighting, yielding a matrix size of 384 × 384 × 11.

Each frame was subdivided into four motion states from inspiration to expiration for both XD-GRASP and RACER-GRASP (25 spokes/motion state) during the reconstruction of the phantom and liver datasets. GROG gridding was implemented to accelerate RACER-GRASP in the liver dataset reconstruction. The end-expiration state was selected in the reference and three motion-corrected schemes for both datasets to ensure a fair comparison. Multiple reconstructions for the proposed L+S with soft weighting scheme were performed on the liver dataset, incorporating shifted soft weighting matrices. The shift step size for the soft weighting matrix was set to eight spokes along the motion dimension, and 12 motion states were reconstructed.

Additional reconstructions were conducted with XD-GRASP, RACER-GRASP, and the proposed method with temporal resolutions of 96 spokes/frame (∼12s/frame), 64 spokes/frame (∼8s), and 32 spokes/frame (∼4s) at the end-expiration state.

The optimization in three GRASP-based schemes was solved using NLCG with 24 iterations. The iteration for ISTA and optimized FISTA was set to 20 and used to solve the optimization problems in L+S decomposition and L+S with soft weighting, respectively. All reconstructions were performed using MATLAB 2022b on an Intel Core i7-10700 PC with a 2.9 GHz processor, and each scheme's reconstruction efficiency was evaluated through 10 repetitions to ensure an accurate assessment.

G. RECONSTRUCTION PARAMETER DESIGN

The performance of DCE-MRI reconstruction schemes is highly dependent on the design of the weighting factor for temporal sparsity constraints. To optimize the regularization parameter for GRASP, XD-GRASP, RACER-GRASP, L+S decomposition, and L+S with soft weighting, a series of reconstructions were performed using these five frameworks with varying λ_T values ranging from $0.1 \times M_s$ to $0.8 \times M_s$, where M_s represents the maximum magnitude of the directly reconstructed image series by the multi-coil NUFFT operator. The variation step size of λ_T was set to $0.05 \times M_s$. Two experienced radiologists were invited to assess the image reconstructed by all five schemes across different λ_T values. An optimized value $\lambda_T = 0.4 \times M_s$ was implemented for all reconstruction schemes.

The motion suppression parameters for XD-GRASP and RACER-GRASP follow their initial setups. In the proposed method, the weighting function parameters n_1 and n_2 were tailored to 23 and 97, respectively, yielding a soft weighting matrix with a seamless transition between the target and other motion states. The constant parameter C was set to 1/64, effectively alleviating the under-sampling ratio and maintaining motion suppression.

III. RESULTS AND DISCUSSION

A. MOTION CORRECTION AND RECONSTRUCTION EFFICIENCY

Figure 4 presents three representative contrast phases of simulated phantom images reconstructed using GRASP, L+S decomposition, XD-GRASP, RACER-GRASP, and the proposed L+S with soft weighting. All the reconstruction schemes successfully suppressed under-sampled streaking artifacts. However, significant motion blurring was obtained in standard GRASP and L+S decomposition. In comparison, XD-GRASP, RACER-GRASP, and the proposed method exhibited reduced motion blurring artifacts.

A comparison of reference to five reconstruction schemes in the zoomed view of a motion region at the end-expiration state in the venous phase is shown in Figure 5. The motion-corrected GRASP schemes effectively suppressed motion blurring. However, due to the excessive AF induced by motion subdivision, reconstructed images using XD-GRASP show relatively low SNR and some residual streaking artifacts. By combining motion states with specific weighting factors, RACER-GRASP alleviated the AF and achieved better image quality than XD-GRASP. The proposed method demonstrates superior motion suppression and image quality simultaneously. Error maps calculated from the five schemes indicated that the proposed method produced fewer errors than XD-GRASP and RACER-GRASP.

Figure 6 and Table 1 summarize the reconstruction performance of the different schemes in reconstructing the phantom dataset. The soft weighting matrix had minimal impact on the iteration cycle time in the L+S decomposition model

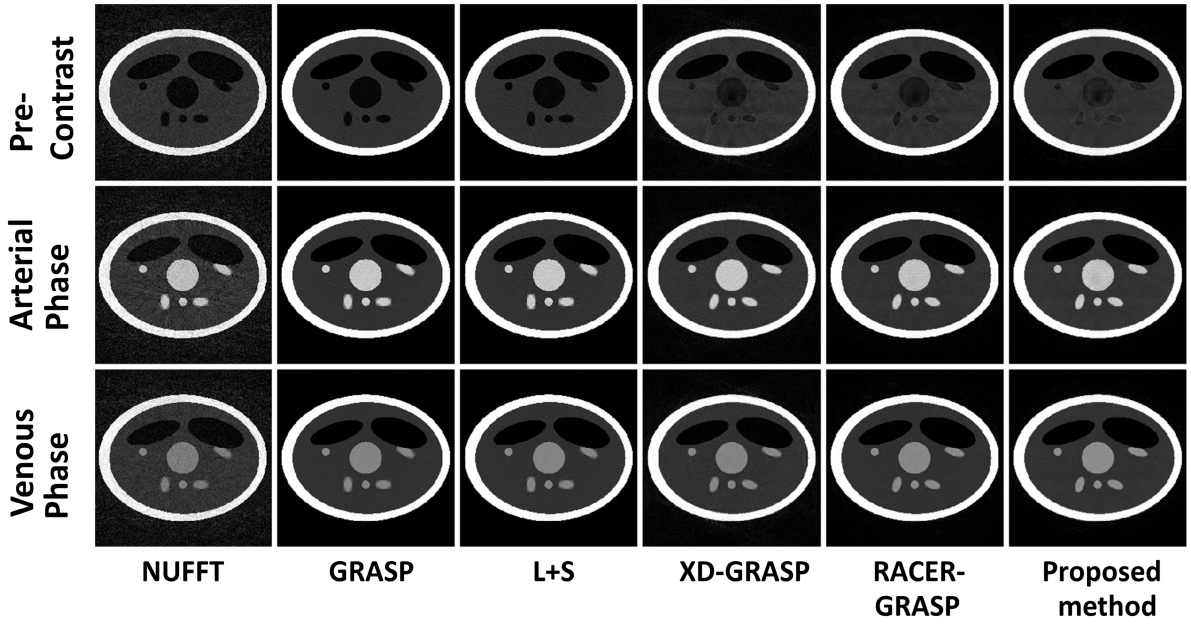

FIGURE 4. A comparison of 6 reconstruction schemes in three representative phase contrasts at the end-expiration state in the phantom dataset. All the image series were reconstructed at AF= 12 and 100 spokes/frame. Significant motion blurring was observed in NUFFT, GRASP, and L+S decomposition. All XD-GRASP, RACER-GRASP, and L+S with soft weighting compressed motion blurring effectively. Some residual streaking artifacts were obtained at the edge of the phantom in XD-GRASP.

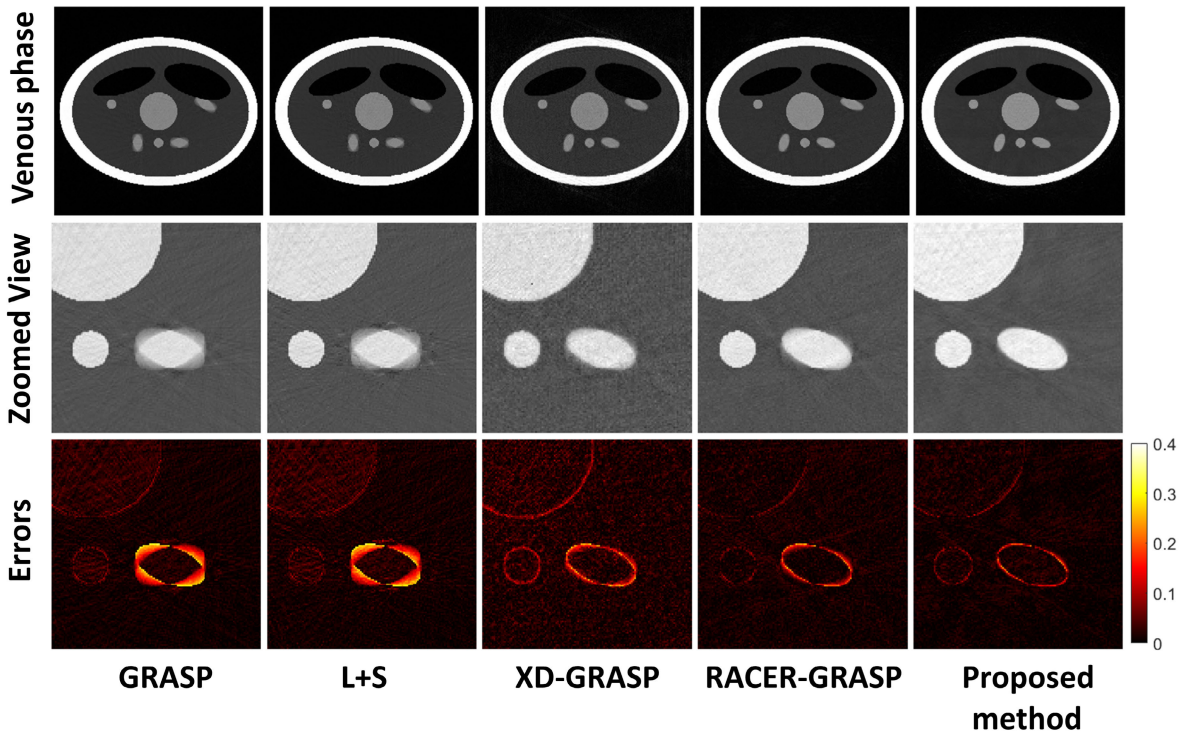

FIGURE 5. A comparison of 5 different reconstruction schemes in the venous phase at the end-expiration stage in the phantom dataset. Three rows of image series correspond to the venous phase image, the zoomed view of a motion region in the venous phase, and the error map in these reconstruction schemes. Significant motion errors were obtained in GRASP and L+S decomposition. L+S with soft weighting shows fewer residual motion artifacts than XD-GRASP and RACER-GRASP. Minimum correction errors were achieved by L+S with soft weighting.

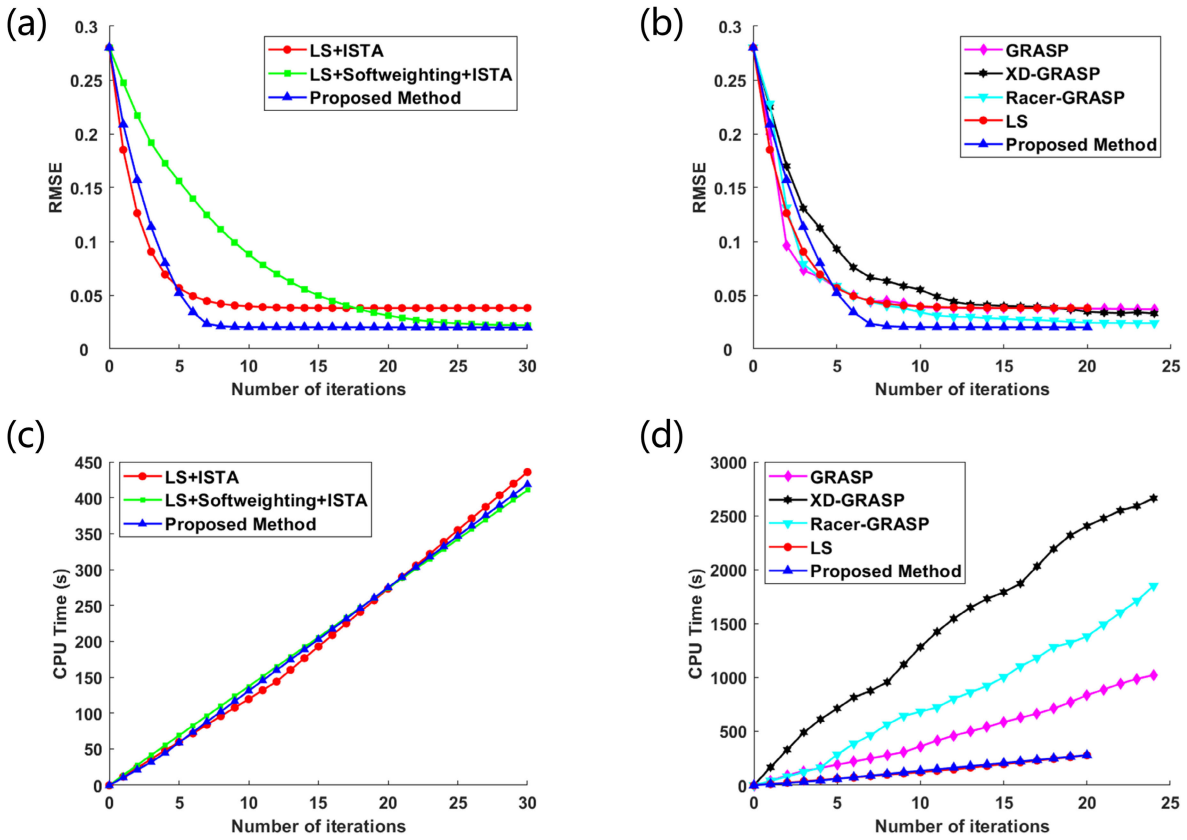

FIGURE 6. A comparison of reconstruction efficiency of different frameworks in reconstructing the phantom dataset. (a) The curve of RMSE versus iteration number for venous phase image reconstructed with three L+S-based frameworks. The proposed method, L+S with soft weighting matrix and FISTA, shows the highest convergence efficiency. (b) The curve of the RMSE versus iteration number for venous phase image reconstructed with different frameworks. (c) The curve of CPU computation time versus iteration number for phantom image series reconstructed with three L+S-based frameworks. (d) The curve of CPU computation time versus iteration number for phantom image series reconstructed with different frameworks.

TABLE 2. Mean DCE signal, reconstruction time, and RMSE of the different reconstruction schemes in reconstructing the phantom dataset. Minimum motion-corrected errors were obtained using the proposed method. Two L+S-based frameworks show much higher reconstruction efficiency than the GRASP-based frameworks. Soft weighting and FISTA introduce a negligible computation burden in the L+S model. The proposed method also shows a higher dynamic contrast signal than other motion-corrected reconstruction schemes.

Reconstruction Scheme	Mean DCE Signal	Reconstruction Time (s)	RMSE
Reference	0.600	-	-
GRASP	0.529	1018.933	0.037
XD-GRASP	0.476	2661.741	0.033
RACER-GRASP	0.464	1847.342	0.024
L+S decomposition	0.481	273.278	0.038
Proposed method	0.528	275.356	0.020

but did reduce convergence speed. The application of the FISTA algorithm in the L+S with soft weighting significantly improves the convergence speed and maintains the short iteration cycle time. Using the selected motion section in the reference as a benchmark, the RMSE values for GRASP, L+S decomposition, XD-GRASP, RACER-GRASP, and L+S with soft weighting were 0.037, 0.038, 0.033, 0.024 and 0.020 respectively, demonstrating the feasibility of the

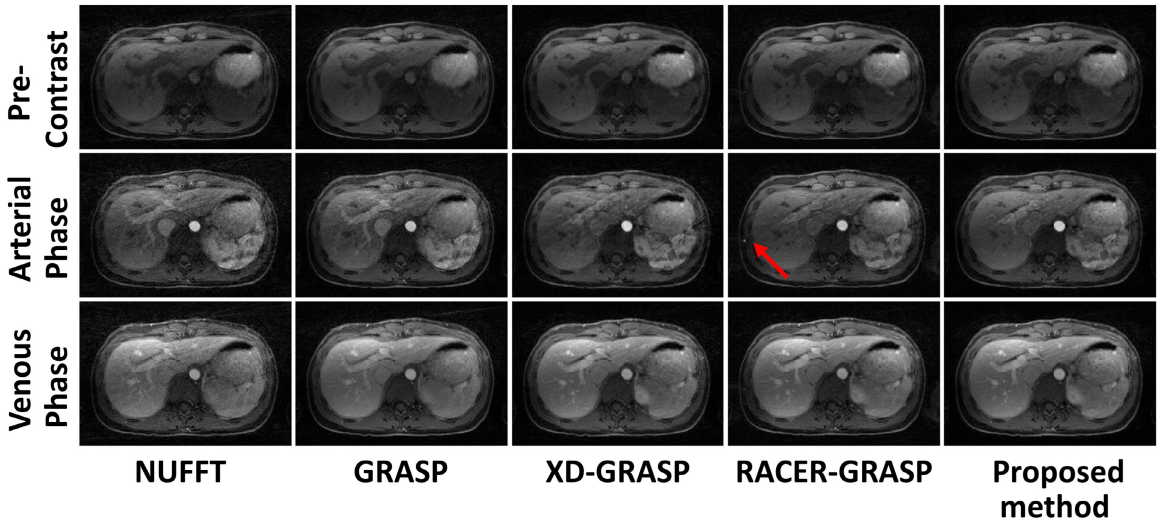

FIGURE 7. A comparison of different reconstruction schemes in three representative phases with respiratory motion in the liver DCE-MRI dataset with a temporal resolution of 100 spokes/frame. The reconstruction period for GRASP, XD-GRASP, RACER-GRASP, and the proposed method is 170.436 s, 560.524 s, 106.012 s, and 58.315 s, respectively. GRASP suffered significant motion-blurring artifacts. XD-GRASP compressed motion blurring but some residual streaking artifacts remained. RACER-GRASP and L+S with soft weighting compressed the motion blurring and achieved better image quality than XD-GRASP. Unexpected convolution artifacts were obtained in RACER-GRASP (labeled by red arrow).

proposed computer simulation framework for quantitatively evaluating the motion correction. The proposed method achieved the lowest motion error, highlighting the robustness of the soft weighting approach for motion suppression. GRASP exhibited low reconstruction efficiency, requiring approximately 15 minutes to complete the computation. The motion state subdivision increases computation time for XD-GRASP and RACER-GRASP, resulting in much worse reconstruction efficiency. The reconstruction time for L+S decomposition and the proposed method was 273.278 s and 275.356 s, respectively. The additional computation cost introduced by the soft weighting matrix and FISTA remained negligible compared to the motion subdivision. As a result, L+S with soft weighting demonstrated much higher reconstruction efficiency than XD-GRASP and RACER-GRASP.

Figure 7 compares different reconstruction schemes for the liver dataset at the end-expiration state. GRASP still exhibited significant motion blurring, while XD-GRASP and RACER-GRASP efficiently reduced motion blurring by employing motion subdivisions. Some residual streaking artifacts were observed in XD-GRASP, while fewer artifacts were presented in RACER-GRASP and the proposed method. However, RACER-GRASP with GROG introduced some convolution artifacts.

Figure 8 presents a zoomed view of the liver section in three representative phases for XD-GRASP, RACER-GRASP, and the proposed method. Less motion blurring was observed in RACER-GRASP, whereas the proposed L+S with soft weighting method demonstrated the best tissue details and motion suppression, particularly in the arterial phase. The average reconstruction time for GRASP, XD-GRASP, RACER-GRASP, and L+S with soft weighting was 170.436 s, 560.524 s, 106.012 s, and 58.315 s, respectively. Although GROG improved the reconstruction efficiency of RACER-GRASP significantly, it introduced unexpected convolutional artifacts. The proposed method achieved the highest reconstruction efficiency without GROG acceleration.

Figure 9 illustrates an additional reconstruction of the proposed method with 12 motion states between inspiration and expiration. By shifting the soft weighting matrix with a small step size along the motion dimension, the proposed method reconstructed the image series at both high temporal and motion resolutions, enabling the exploration of liver tissue variations caused by respiratory motion in DCE-MRI. The transparent display of tissue variation throughout a respiratory cycle may provide valuable information for diagnosing diseases related to respiratory function.

Figure 10 compares different motion-corrected methods in the venous phases at the end-expiration state in the liver DCE-MRI dataset with temporal resolutions of 96 spokes/frame, 64 spokes/frame, and 32 spokes/frame. XD-GRASP failed at higher temporal resolution due to the excessive under-sampling ratio and therefore is not shown. Both RACER-GRASP and the proposed method supported motion-corrected DCE-MRI reconstruction at high temporal resolutions. Better background structures and fewer image degradations were observed by the proposed method.

B. PERFORMANCE ANALYSIS

The golden angle radial sampling pattern repeatedly acquires the k-space center, providing an averaging effect

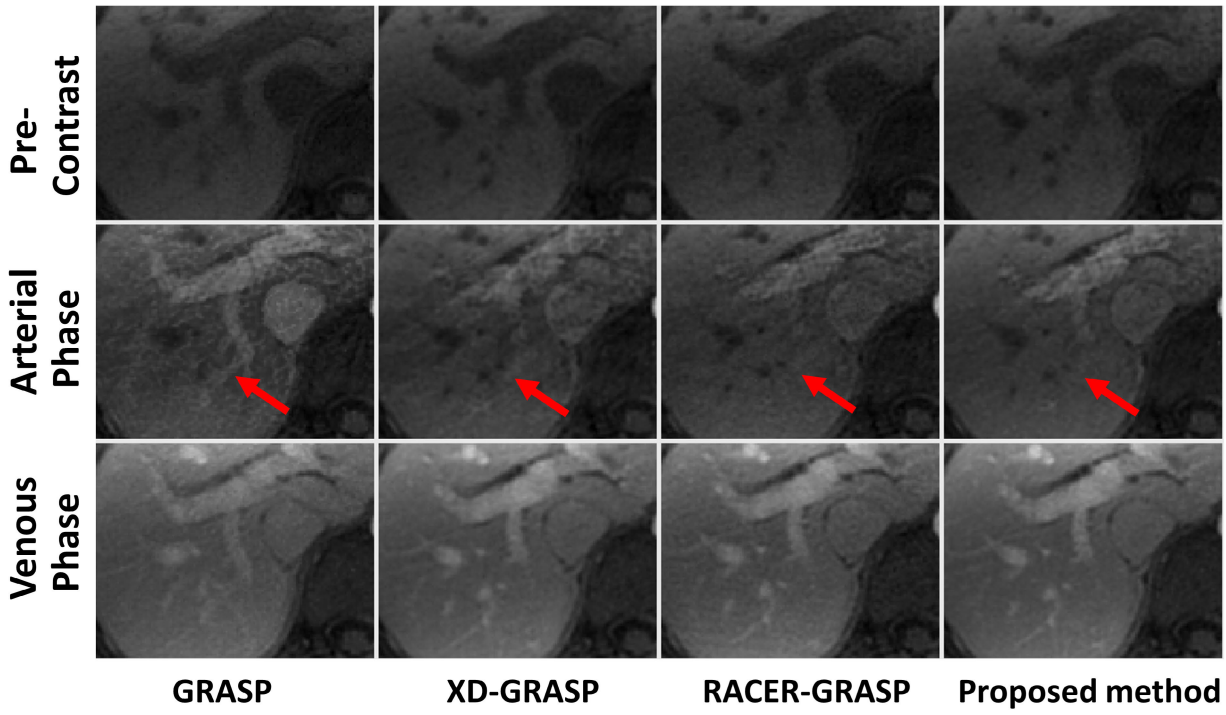

FIGURE 8. A zoomed view of the liver section in three representative phases reconstructed by GRASP, XD-GRASP, RACER-GRASP, and L+S with soft weighting. Respiratory motion leads to blurring artifacts while unclear vessel structures were obtained in the GRASP. Minimum motion artifacts were obtained in the proposed method, especially in the arterial phase (labeled by red arrows).

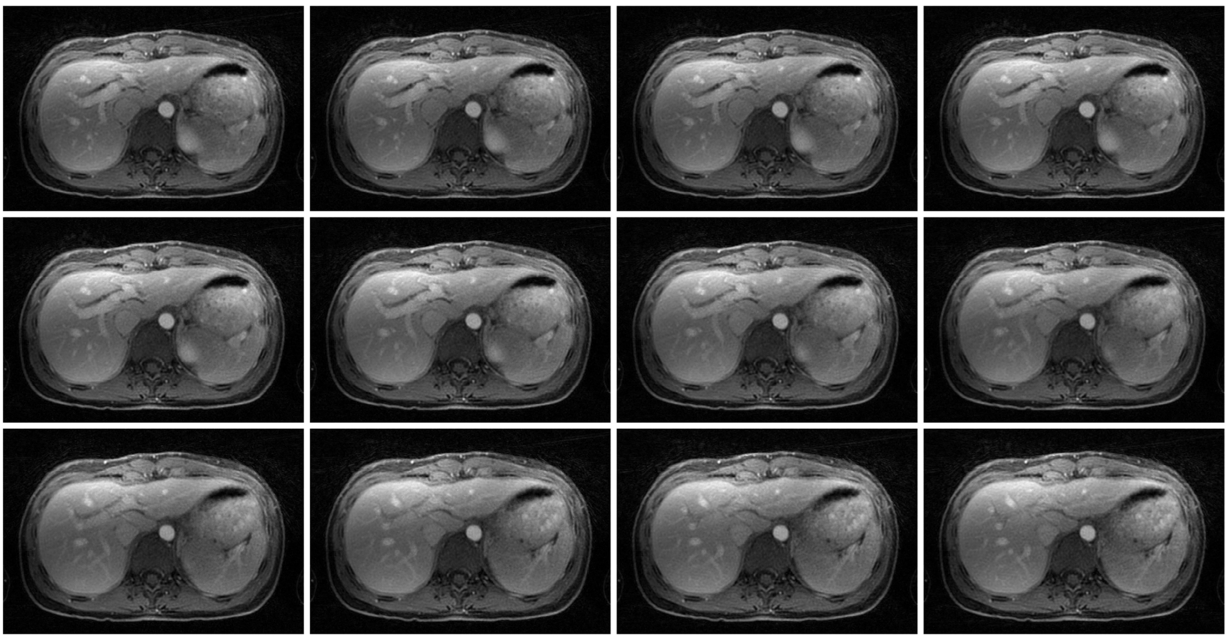

FIGURE 9. 12 motion states reconstructed by the proposed method with shifted respiratory weighting factors in the liver DCE-MRI dataset. Feasible motion states reconstruction was certified. The image series with high motion resolution explores the tissue variation caused by respiratory motion.

and suppressing motion artifacts. However, periodic rigid motions can still lead to blurring artifacts, degrading the image quality in DCE-MRI. Both commonly used DCE-MRI reconstruction frameworks, GRASP and L+S decomposition, are significantly influenced by rigid motion, resulting in blurred vessel details in the reconstructed images.

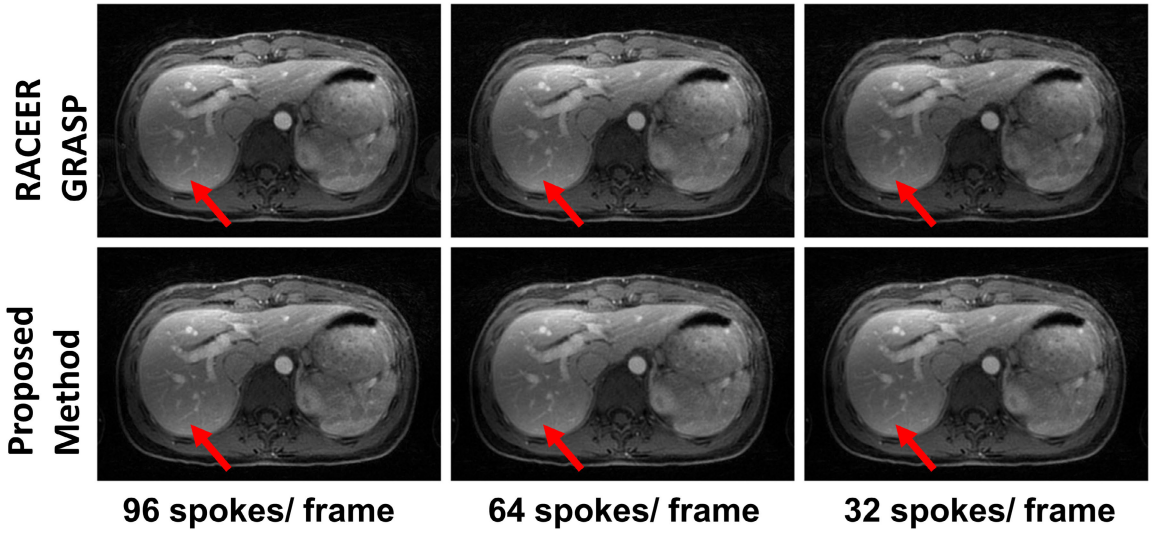

FIGURE 10. A comparison of different motion-corrected methods in reconstructing the liver DCE-MRI dataset in venous phases at end-expiration state with temporal resolutions of 96 spokes/frame(∼ 12s/frame), 64 spokes/frame (∼ 8s/frame), and 32 spokes/frame (∼ 12s/frame). XD-GRASP shows failed reconstruction at higher temporal resolution and is not displayed here. The increased temporal resolution degraded the motion suppression quality in RACER-GRASP, while less degradation was obtained using the proposed method. The proposed method provides improved tissue structures (labeled by red arrow) at a much higher temporal resolution.

XD-GRASP and RACER-GRASP were developed to improve conventional GRASP by reducing motion blurring through additional motion state subdivisions. By utilizing the inherent self-guiding property of the stack-of-stars sampling scheme, motion signals can be accurately estimated without requiring extra hardware devices. XD-GRASP and RACER-GRASP resorted acquired spokes within each time frame based on the estimated motion signal and subdivided them into multiple motion state groups. This approach minimizes the difference in motion states among spokes within the same group. XD-GRASP and RACER-GRASP provide rich motion state information in addition to the temporal dimension information.

XD-GRASP employs two TV operators to simultaneously explore temporal sparsity among time frames and motion sparsity among motion state groups. By reconstructing each motion state individually, XD-GRASP effectively suppresses motion blurring and provides additional motion state information. However, the k-space in each temporal frame is already highly under-sampled, and the extra motion state subdivision further increases the under-sampling ratio. The number of spokes within a time frame must be increased to support motion subdivision. Consequently, the temporal resolution of the reconstructed image series is typically limited in the motion-resolved methods. Despite efforts to control the AF by reducing the temporal resolution, residual streaking artifacts are frequently observed in XD-GRASP.

To mitigate streaking artifacts caused by an excessive under-sampling ratio, RACER-GRASP explores the temporal sparsity of each motion state individually and combines these motion states using specific weighting factors. By carefully adjusting these weighting factors, the end-expiration state can be locked as the output, effectively suppressing motion blurring and streaking artifacts. Compared to XD-GRASP, RACER-GRASP is significantly less affected by motion state subdivision regarding reconstruction temporal resolution. Multiple motion states can be reconstructed in RACER-GRASP by adjusting the weighting factor design for each motion state. However, RACER-GRASP shows poorer reconstruction quality in intermediate motion states due to the limitations of the weighting function design.

In addition to motion correction, reconstruction efficiency is crucial for online clinical applications. The reconstruction efficiency of GRASP is relatively low due to repetitive gridding and de-gridding operations in NLCG. This efficiency is further reduced in XD-GRASP and RACER-GRASP due to motion subdivision, which significantly increases the computation burden in NLCG. Motion subdivision often extends the reconstruction process to dozens of minutes. The reconstruction efficiency of GRASP-based schemes can be improved by employing the GROG algorithm, which converts non-Cartesian-based datasets into Cartesian-based datasets before iterative reconstruction, thereby reducing the computational cost of gridding. However, the performance of GROG interpolation heavily depends on reference kernel training, which may introduce unexpected convolutional artifacts during reconstruction.

Compared to GRASP-based schemes, L+S-based schemes can provide much higher reconstruction efficiency in DCE-MRI. A soft weighting matrix has been introduced with L+S decomposition to suppress motion blurring and maintain high reconstruction efficiency simultaneously. The proposed L+S with soft weighting implements a soft weighting matrix to control the contribution of spokes acquired at different

motion states within each time frame. Using a sigmoid function, the matrix coefficients provide a smooth transition between the stopband and passband. The motion state of the output image series can be accurately locked with less interference from other motion states, achieving better motion suppression. The additional under-sampling ratio introduced by the soft weighting matrix is typically less than that by motion subdivision, resulting in fewer streaking artifacts in the proposed method.

To accelerate convergence and further reduce streaking artifacts, an optimized FISTA algorithm is employed to find the optimal solution for the proposed model. During the first two iterations of FISTA, the soft-weighting matrix remains inactive, allowing the initial image series to be reconstructed with fewer streaking artifacts for the subsequent iterative reconstruction. Under the influence of the soft weighting matrix, the time series gradually converges toward the target motion state during the remaining iterations. Ultimately, the proposed method achieves motion-corrected reconstruction with significantly higher temporal resolution in DCE-MRI than conventional motion-resolved methods.

The soft weighting matrix has minimal effect on the iteration cycle time in ISTA but does reduce the convergence speed. Applying the FISTA algorithm to the L+S with soft weighting significantly improves the convergence speed while the short iteration cycle time of L+S decomposition is maintained. Moreover, the number of gridding and de-gridding steps in FISTA is considerably less than that of NLCG. As a result, the proposed L+S with soft weighting achieves significantly higher reconstruction efficiency than GRASP-based schemes, even when GRASP schemes are accelerated using GROG gridding.

Besides motion suppression and reconstruction efficiency, another significant advantage of the proposed method is its ability to perform feasible motion state reconstruction. The under-sampling ratio often limits the motion state resolution in conventional motion-resolved methods. The motion suppression quality of RACER-GRASP is typically limited at the intermediate state of the motion cycle. By shifting the weighting factors in the soft weighting matrix along the motion dimension, the proposed method can provide abundant motion phase information similar to XD-GRASP but with higher motion state resolution. With a sufficiently small step size, our method can generate a motion animation that captures the entire respiratory motion period. Furthermore, due to the removal of motion subdivision, the proposed method is not constrained by the minimum number of spokes as in XD-GRASP or RACER-GRASP. The proposed L+S with soft weighting demonstrates excellent motion suppression in DCE-MRI with both high temporal resolution and improved motion state resolution.

The motion suppression performance of DCE-MRI conventional reconstruction schemes is typically evaluated visually by experienced radiologists. Acquiring a fully sampled DCE-MRI dataset as the reference is challenging, and there are no standard evaluation criteria for quantifying the performance of different reconstruction schemes. Therefore, a computer simulation framework was developed in this work. The advantage of computer simulation is that the ground truth, such as motion phases, can be simulated and accurately obtained. The motion suppression of the proposed method and other reconstruction schemes can be compared and evaluated using metrics like error maps. The proposed method achieved the minimum RMSE, demonstrating the feasibility of this new computer simulation framework for quantitatively assessing motion suppression.

IV. CONCLUSION

This study proposes a new motion-corrected reconstruction framework, L+S with soft weighting, for free-breathing liver DCE-MRI. By combining low-rank decomposition, a soft weighting matrix, and FISTA, the proposed method enables rapid DCE-MRI reconstruction with improved motion suppression, high temporal resolution, and rich motion state information compared to XD-GRASP and RACER-GRASP. The proposed method provides improved image quality with exceptionally high motion state resolution, demonstrating its potential for detecting liver structural and functional disorders in clinical settings.

REFERENCES

[1] A. R. Padhani, "Dynamic contrast-enhanced MRI in clinical oncology: Current status and future directions," *J. Magn. Reson. Imag.*, vol. 16, no. 4, pp. 407–422, Oct. 2002.

[2] M. Usman, D. Atkinson, F. Odille, C. Kolbitsch, G. Vaillant, T. Schaeffter, P. G. Batchelor, and C. Prieto, "Motion corrected compressed sensing for free-breathing dynamic cardiac MRI," *Magn. Reson. Med.*, vol. 70, no. 2, pp. 504–516, Aug. 2013.

[3] S. P. Sourbron and D. L. Buckley, "Classic models for dynamic contrast-enhanced MRI," *NMR Biomed.*, vol. 26, no. 8, pp. 1004–1027, Aug. 2013.

[4] R. M. Mann, C. Kühl, and L. Moy, "Contrast-enhanced MRI for breast cancer screening," *J. Magn. Reson. Imaging.*, vol. 50, no. 2, pp. 377–390, Jan. 2019.

[5] D. Albano et al., "Dynamic contrast-enhanced (DCE) imaging: State of the art and applications in whole-body imaging," *Jpn. J. Radiol.*, vol. 40, no. 4, pp. 341–366, Apr. 2022.

[6] A. Zhou, J. R. Leach, C. Zhu, H. Dong, F. Jiang, Y. J. Lee, J. Iannuzzi, W. Gasper, D. Saloner, M. D. Hope, and D. Mitsouras, "Dynamic contrast-enhanced MRI in abdominal aortic aneurysms as a potential marker for disease progression," *J. Magn. Reson. Imag.*, vol. 58, no. 4, pp. 1258–1267, Feb. 2023.

[7] H. Chandarana, L. Feng, T. K. Block, A. B. Rosenkrantz, R. P. Lim, J. S. Babb, D. K. Sodickson, and R. Otazo, "Free-breathing contrast-enhanced multiphase MRI of the liver using a combination of compressed sensing, parallel imaging, and golden-angle radial sampling," *Investigative Radiol.*, vol. 48, no. 1, pp. 10–16, Jan. 2013.

[8] L. Feng, R. Grimm, K. T. Block, H. Chandarana, S. Kim, J. Xu, L. Axel, D. K. Sodickson, and R. Otazo, "Golden-angle radial sparse parallel MRI: Combination of compressed sensing, parallel imaging, and golden-angle radial sampling for fast and flexible dynamic volumetric MRI," *Magn. Reson. Med.*, vol. 72, no. 3, pp. 707–717, Sep. 2014.

[9] Z. Zhou, F. Han, L. Yan, D. J. J. Wang, and P. Hu, "Golden-ratio rotated stack-of-stars acquisition for improved volumetric MRI," *Magn. Reson. Med.*, vol. 78, no. 6, pp. 2290–2298, Dec. 2017.

[10] A. B. Rosenkrantz, C. Geppert, R. Grimm, T. K. Block, C. Glielmi, L. Feng, R. Otazo, J. M. Ream, M. M. Romolo, S. S. Taneja, D. K. Sodickson, and H. Chandarana, "Dynamic contrast-enhanced MRI of the prostate with high spatiotemporal resolution using compressed sensing, parallel imaging, and continuous golden-angle radial sampling: Preliminary experience," *J. Magn. Reson. Imag.*, vol. 41, no. 5, pp. 1365–1373, May 2015.

[11] L. Feng, "Golden-angle radial MRI: Basics, advances, and applications," *J. Magn. Reson. Imag.*, vol. 56, no. 1, pp. 45–62, Jul. 2022.
[12] L. Feng, L. Axel, H. Chandarana, K. T. Block, D. K. Sodickson, and R. Otazo, "XD-GRASP: Golden-angle radial MRI with reconstruction of extra motion-state dimensions using compressed sensing," *Magn. Reson. Med.*, vol. 75, no. 2, pp. 775–788, Feb. 2016.
[13] L. Feng, C. Huang, K. Shanbhogue, D. K. Sodickson, H. Chandarana, and R. Otazo, "RACER-GRASP: Respiratory-weighted, aortic contrast enhancement-guided and coil-unstreaking golden-angle radial sparse MRI," *Magn. Reson. Med.*, vol. 80, no. 1, pp. 77–89, Jul. 2018.
[14] Z. Li, C. Huang, A. Tong, H. Chandarana, and L. Feng, "Kz-accelerated variable-density stack-of-stars MRI," *Magn. Reson. Imag.*, vol. 97, pp. 56–67, Apr. 2023.
[15] L. Chen, J. Xu, D. Liu, B. Ji, J. Wang, X. Zeng, J. Zhang, and L. Feng, "High-resolution free-breathing hepatobiliary phase MRI of the liver using XD-GRASP," *Magn. Reson. Imag.*, vol. 109, pp. 42–48, Jun. 2024.
[16] L. Feng, Q. Wen, C. Huang, A. Tong, F. Liu, and H. Chandarana, "GRASP-Pro: imProving GRASP DCE-MRI through self-calibrating subspace-modeling and contrast phase automation," *Magn. Reson. Med.*, vol. 83, no. 1, pp. 77–89, Aug. 2019.
[17] L. Chen, X. Zeng, B. Ji, D. Liu, J. Wang, J. Zhang, and L. Feng, "Improving dynamic contrast-enhanced MRI of the lung using motion-weighted sparse reconstruction: Initial experiences in patients," *Magn. Reson. Imag.*, vol. 68, pp. 36–44, May 2020.
[18] H. Haji-Valizadeh, L. Feng, L. E. Ma, D. Shen, K. T. Block, J. D. Robinson, M. Markl, C. K. Rigsby, and D. Kim, "Highly accelerated, real-time phase-contrast MRI using radial k-space sampling and GROG-GRASP reconstruction: A feasibility study in pediatric patients with congenital heart disease," *NMR Biomed.*, vol. 33, no. 5, p. 4240, Jan. 2020.
[19] F. Aamir, H. Bhatti, I. Aslam, F. Najeeb, and H. Omer, "GROG-pCS: GRAPPA operator gridding with CS-based p-thresholding for under-sampled radially encoded MRI," *Int. J. Emerg. Multidisciplinaries, Biomed. Clin. Res.*, vol. 1, no. 1, pp. 1–16, Jun. 2023.
[20] T. Benkert, Y. Tian, C. Huang, E. V. R. DiBella, H. Chandarana, and L. Feng, "Optimization and validation of accelerated golden-angle radial sparse MRI reconstruction with self-calibrating GRAPPA operator gridding," *Magn. Reson. Med.*, vol. 80, no. 1, pp. 286–293, Jul. 2018.
[21] Z. Ding, Z. Cheng, H. She, B. Liu, Y. Yin, and Y. P. Du, "Dynamic pulmonary MRI using motion-state weighted motion-compensation (MostMoCo) reconstruction with ultrashort TE: A structural and functional study," *Magn. Reson. Med.*, vol. 88, no. 1, pp. 234–238, Apr. 2022.
[22] F. Tan, X. Zhu, M. Chan, M. A. Zapala, S. S. Vasanawala, F. Ong, M. Lustig, and P. E. Z. Larson, "Motion-compensated low-rank reconstruction for simultaneous structural and functional UTE lung MRI," *Magn. Reson. Med.*, vol. 90, no. 3, pp. 1101–1113, Sep. 2023.
[23] C. Mattusch, U. Bick, and F. Michallek, "Development and validation of a four-dimensional registration technique for DCE breast MRI," *Insights Imag.*, vol. 14, no. 1, p. 17, Jan. 2023.
[24] W. Qiu, D. Li, X. Jin, F. Liu, T. D. Nguyen, M. R. Prince, Y. Wang, and P. Spincemaille, "Sliding motion compensated low-rank plus sparse (SMC-LS) reconstruction for high spatiotemporal free-breathing liver 4D DCE-MRI," *Magn. Reson. Imag.*, vol. 58, pp. 56–66, May 2019.
[25] C. Ariyurek, A. Koçanaoğullari, O. Afacan, and S. Kurugol, "Motion-compensated image reconstruction for improved kidney function assessment using dynamic contrast-enhanced MRI," *NMR Biomed.*, vol. 37, no. 6, p. 5116, Jun. 2024.
[26] Z. Miller, L. Torres, S. Fain, and K. Johnson, "Motion compensated extreme MRI: Multi-scale low rank reconstructions for highly accelerated 3D dynamic acquisitions (MoCo-MSLR)," Apr. 2024.
[27] L. Feng, "4D golden-angle radial MRI at subsecond temporal resolution," *NMR Biomed.*, vol. 36, no. 2, p. 4844, Feb. 2023.
[28] S. G. Lingala, Y. Hu, E. DiBella, and M. Jacob, "Accelerated dynamic MRI exploiting sparsity and low-rank structure: K-t SLR," *IEEE Trans. Med. Imag.*, vol. 30, no. 5, pp. 1042–1054, May 2011.
[29] R. Otazo, E. Candès, and D. K. Sodickson, "Low-rank plus sparse matrix decomposition for accelerated dynamic MRI with separation of background and dynamic components," *Magn. Reson. Med.*, vol. 73, no. 3, pp. 1125–1136, Mar. 2015.
[30] K. H. Jin, D. Lee, and J. C. Ye, "A general framework for compressed sensing and parallel MRI using annihilating filter based low-rank Hankel matrix," *IEEE Trans. Comput. Imag.*, vol. 2, no. 4, pp. 480–495, Dec. 2016.
[31] A. Beck and M. Teboulle, "A fast iterative shrinkage-thresholding algorithm for linear inverse problems," *SIAM J. Imag. Sci.*, vol. 2, no. 1, pp. 183–202, Jan. 2009.
[32] J. Zhang, "Improved ultrashort time echo and dynamic contrast enhancement magnetic resonance imaging based on stack-of-stars golden angle radial sampling scheme," Ph.D. dissertation, Dept. Electr. Electron. Eng., Univ. Nottingham Ningbo China, Ningbo, China, 2022.
[33] T. Zhang, J. Y. Cheng, Y. Chen, D. G. Nishimura, J. M. Pauly, and S. S. Vasanawala, "Robust self-navigated body MRI using dense coil arrays," *Magn. Reson. Med.*, vol. 76, no. 1, pp. 197–205, Jul. 2016.
[34] J. Tanner and S. Vary, "Compressed sensing of low-rank plus sparse matrices," *Appl. Comput. Harmon. Anal.*, vol. 64, pp. 254–293, May 2023.
[35] J. Zhang, F. Najeeb, X. Wang, P. Xu, H. Omer, J. Zheng, J. Zhang, S. Francis, P. Glover, R. Bowtell, and C. Wang, "Improved dynamic contrast-enhanced MRI using low rank with joint sparsity," *IEEE Access*, vol. 10, pp. 121193–121203, 2022.
[36] J. Liang, T. Luo, and C. B. Schonlieb, "Improving 'fast iterative shrinkage-thresholding algorithm': Faster, smarter, and greedier," *SIAM J. Sci. Comput.*, vol. 44, no. 3, pp. 1069–1091, 2022.
[37] J. Huang, L. Wang, and Y. Zhu, "Compressed sensing MRI reconstruction with multiple sparsity constraints on radial sampling," *Math. Problems Eng.*, vol. 2019, no. 1, pp. 1–14, Feb. 2019.
[38] D. O. Walsh, A. F. Gmitro, and M. W. Marcellin, "Adaptive reconstruction of phased array MR imagery," *Magn. Reson. Med.*, vol. 43, no. 5, pp. 682–690, May 2000.

JICHANG ZHANG received the B.S. degree in electrical and electronic engineering, the M.S. degree in electronic communication and computer engineering, and the Ph.D. degree from the University of Nottingham, Ningbo, China, in 2015, 2016, and 2022, respectively. His research interests include dynamic MRI, pulse sequence development, and acceleration techniques for image reconstruction.

FAISAL NAJEEB received the Ph.D. degree in electrical engineering (medical imaging) from COMSATS University Islamabad, Pakistan, in 2021. He did his postgraduate research with the SPMIC University of Nottingham, U.K., as a part of his Ph.D. research, in 2020. He is currently an Assistant Professor with the Electrical and Computer Engineering Department, COMSATS University Islamabad, where he is also an active member of the Medical Image Processing Research Group (MIPRG). His research interests include MR image reconstruction, multi modal image translation (e.g., CT to MRI and T1 to T2) using deep learning techniques, and MR image super resolution.

YULIN WANG received the B.S. degree in electrical and electronic engineering from the University of Nottingham, Ningbo, China, in 2020, where she is currently pursuing the Ph.D. degree in electrical and electronic engineering. Her research interests include MRI acoustic noise reduction, pulse sequence development, T1 mapping, and image reconstruction.

XINPEI WANG received the B.S. and Ph.D. degrees in electrical and electronic engineering from the University of Nottingham, Ningbo, China, in 2017 and 2022, respectively. His research interests include MR image reconstruction, T1 mapping, pulse sequence development, new hyperpolarizer techniques, and hyperpolarized Xe application.

PENGFEI XU received the B.E. degree in automation from Xian Technological University, Xi'an, China, in 2015, and the M.S. degree in control science and engineering from the University of Science and Technology Beijing, Beijing, China, in 2018. She is currently pursuing the Ph.D. degree in electrical and electronic engineering with the University of Nottingham, Ningbo, China. Her research interests include MRI sequences, image reconstruction, and oxygen-enhanced lung MRI.

HAMMAD OMER received the M.S. and Ph.D. degrees from the Imperial College London, U.K. He is currently the Group Leader of the Medical Image Processing Research Group (MIPRG), COMSATS University Islamabad. He has more than ten students have completed Ph.D. under his supervision in MRI imaging. His research interests include MRI image reconstruction, diffusion-weighted MRI, cardiac MRI, and AI-based MR image reconstruction. He is also working on the optimization of medical image reconstruction algorithms for an efficient implementation on FPGA and GPUs.

JIANJUN ZHENG received the B.M. degree in clinical medicine from Zhejiang University, China, in 2003, and the M.S. degree from The University of Hong Kong, in 2007. He is currently a Doctoral Tutor with Ningbo University, China. He is also the Director of Ningbo Hwamei Hospital, University of Chinese Academy of Sciences (Ningbo Second Hospital). With 28 years of clinical experience, he is an Expert in the early diagnosis of tumors, multidisciplinary collaboration, the formulation of individualized diagnosis, and treatment plans. His research interests include clinical imaging, molecular imaging in the tumor, cardiovascular direction, and new imaging materials.

JINGFENG ZHANG received the Ph.D. degree in image medicine and nuclear medicine from the Tongji Medical College, Huazhong University of Science and Technology, in 2005. He is currently a Chief Physician of the Radiology Department, the Chief of the Education Section, and the Director of the Diagnosis and Treatment Center, Ningbo Hwamei Hospital, University of Chinese Academy of Sciences (Ningbo Second Hospital). His research interests include imaging diagnosis and interventional treatment of complicated diseases, intelligent imaging, and intelligent medical education.

SUE FRANCIS is currently a Professor in physics with the Faculty of Science, University of Nottingham. Her research interest includes developing magnetic resonance imaging (MRI) methods for biomedical applications. This has included the application and development of functional magnetic resonance imaging (fMRI) techniques in neuroscience and the development of quantitative MRI methods. She has developed/implemented arterial spin labeling (ASL) methods to measure blood flow and blood volume non-invasively in the brain.

PAUL GLOVER is currently an Associate Professor in physics with the Faculty of Science, University of Nottingham, U.K. His research interests include developments and applications of magnetic resonance imaging which include the design of radio-frequency probes to generate the required excitation fields, the safety of magnetic fields, and their interaction with the human body.

RICHARD BOWTELL received the degree in natural science from the University of Cambridge and the Ph.D. degree from the University of Nottingham, in 1984. He is currently the Head of the School of Physics and Astronomy, University of Nottingham. His research is carried out at the Sir Peter Mansfield Magnetic Resonance Centre. His research interests include developing improved equipment and techniques for magnetic resonance imaging and applying them in biomedical studies and spatio-topic mapping of human–brain function using ultra-high field MRI.

CHENGBO WANG received the B.S. and M.S. degrees in biomedical engineering from Tsinghua University and the Ph.D. degree from the University of Virginia, in 2007. He is currently an Associate Professor with the University of Nottingham, Ningbo, China. His research interests include the theoretical and experimental development of new magnetic resonance imaging techniques to meet the research and clinical needs of the medical and biomedical community, MRI hardware, optimization of the MRI pulse sequences, MRI physics, and hyperpolarized noble-gases MRI.